CHAPTER 98

IRREGULAR WAVE INTERACTION WITH PERMEABLE SLOPES

Nobuhisa Kobayashi[1], and Andojo Wurjanto[2]

ABSTRACT: A one-dimensional, time-dependent numerical model is developed to simulate the flow over a rough permeable slope as well as the flow inside a permeable underlayer of arbitrary thickness for specified normally-incident irregular waves. The numerical model has been shown to be capable of predicting the time series and spectral characteristics of the reflected waves and waterline oscillations on a 1:3 rough slope with a thick permeable underlayer. The computed results are examined in detail to quantify the hydrodynamic processes which are difficult to measure in experiments. The computed results for the rough permeable and impermeable slopes are also compared to quantify the differences caused solely by the thick permeable underlayer.

INTRODUCTION

The permeability effects on wave run-up and reflection as well as armor stability have been regarded by previous researchers to be important for the design of highly permeable coastal structures such as berm breakwaters. Our quantitative understanding of the hydrodynamic processes involved with irregular wave interaction with permeable slopes is still rudimentary, although extensive hydraulic model tests have been performed.

Kobayashi and Wurjanto (1990) developed a numerical model for predicting the flow on a rough permeable slope as well as the flow in a thin permeable underlayer for normally incident irregular waves. This numerical model was limited to a thin permeable underlayer because it neglected the region landward of the waterline on the rough slope and the inertia terms in the horizontal momentum equation for the flow in the thin permeable underlayer. This numerical model turned out to be of limited practical use since the permeability effects of the thin permeable underlayer were found to be minor or negligible. Wurjanto and Kobayashi (1992) developed an improved numerical model by eliminating most of the shortcomings of the previous model as explained in the next section.

NUMERICAL MODEL FOR THICK PERMEABLE UNDERLAYER

Fig. 1 shows the symbols used in the improved numerical model where the prime indicates the dimensional variables. In Fig. 1, x' = horizontal coordinate taken to be positive landward with $x' = 0$ at the toe of the slope; z' = vertical coordinate taken to be positive upward with

---

[1]Prof. and Assoc. Dir., Ctr. for Applied Coastal Res., Dept. of Civil Engrg., Univ. of Delaware, Newark, DE 19716.
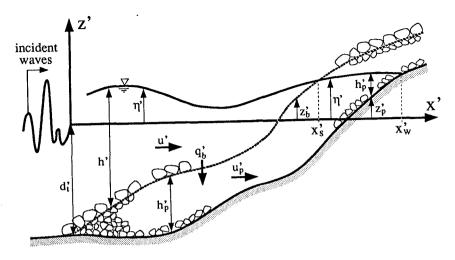[2]Lecturer, Dept. of Civil Engrg., Bandung Inst. of Tech., Jalan Ganesha 10, Bandung 40132, Indonesia.

Figure 1: Definition Sketch for Numerical Model for Thick Permeable Underlayer

$z' = 0$ at the still water level (SWL); $z'_b = z' -$ coordinate of the upper boundary of the permeable underlayer excluding the primary cover layer whose roughness effect is included by the bottom friction factor f' for the flow over the rough slope; $z'_p = z' -$ coordinate of the lower boundary of the permeable underlayer which is assumed impermeable; $d'_t =$ water depth below SWL at $x' = 0$ where it is assumed that $z'_b = z'_p$ at $x' = 0$; $\eta' =$ free surface or water table elevation above SWL; $x'_s = x' -$ coordinate of the upper waterline defined as the location of $\eta' = z'_b$; $x'_w = x'-$ coordinate of the lower waterline defined as the location of $\eta' = z'_p$; $h' =$ water depth above the permeable slope given by $h' = (\eta' - z'_b)$ in the region $0 \leq x' \leq x'_s$; $u' =$ depth-averaged horizontal velocity above the permeable slope; $h'_p =$ water depth inside the permeable underlayer given by $h'_p = (z'_b - z'_p)$ in the region $0 \leq x' \leq x'_s$ and $h'_p = (\eta' - z'_p)$ in the region $x'_s \leq x' \leq x'_w$; $q'_b =$ volume influx per unit horizontal area into the permeable underlayer which is taken to be positive downward; and $u'_p =$ vertically-averaged horizontal discharge velocity inside the permeable underlayer where the actual velocity is given by u'_p/n_p with $n_p =$ porosity of the permeable underlayer.

    Computation is performed using the dimensionless variables and parameters defined as

$$t = \frac{t'}{T'} \; ; \; x = \frac{x'}{T'\sqrt{gH'}} \; ; \; x_s = \frac{x'_s}{T'\sqrt{gH'}} \; ; \; x_w = \frac{x'_w}{T'\sqrt{gH'}} \tag{1}$$

$$z = \frac{z'}{H'} \; ; \; z_b = \frac{z'_b}{H'} \; ; \; z_p = \frac{z'_p}{H'} \; ; \; d_t = \frac{d'_t}{H'} \; ; \; \eta = \frac{\eta'}{H'} \; ; \; h = \frac{h'}{H'} \; ; \; h_p = \frac{h'_p}{H'} \tag{2}$$

$$u = \frac{u'}{\sqrt{gH'}} \; ; \; q_b = \frac{T'q'_b}{p_q H'} \; ; \; u_p = \frac{u'_p}{p_q\sqrt{gH'}} \; ; \; p_q = n_p p_u \tag{3}$$

$$p_u = \left[\frac{n_p}{\beta_0(1-n_p)} \frac{d'_p}{T'\sqrt{gH'}} \right]^{1/2} \quad ; \quad \mu = \frac{\alpha_0(1-n_p)^2\nu}{\beta_0 p_u d'_p \sqrt{gH'}} \tag{4}$$

in which $t' =$ time; T' and $H' =$ characteristic wave period and height used for the normalization, respectively; $g =$ gravitational acceleration; p_q and $p_u =$ dimensionless parameter expressing the order of magnitude of u'_p/u' and $(u'_p/n_p)/u'$, respectively; $\nu =$ kinematic viscosity of the fluid; $d'_p =$ characteristic stone diameter in the permeable underlayer; α_0 and $\beta_0 =$ empirical constant associated with the laminar and turbulent flow resistance, respectively (Madsen and White 1975); and $\mu =$ dimensionless parameter expressing the order of magnitude of the laminar flow resistance as compared to the turbulent flow resistance.

The numerical model of Wurjanto and Kobayashi (1992) computed $m = uh$, $h = (\eta - z_b)$, q_b and $m_p = p_u h_p u_p$ in the region $0 \le x \le x_s$ where $h_p = (z_b - z_p)$, as well as m_p and $h_p = (\eta - z_p)$ in the region $x_s \le x \le x_w$ as a function of t and x using the one-dimensional, time-dependent equations of conservation of mass and x-momentum for the flow fields over and inside the permeable underlayer. It is assumed that m_p and h_p are continuous at $x = x_s$. The initial time $t = 0$ for the computation marching forward in time is taken to be the time when the specified incident wave train arrives at $x = 0$ and there is no wave action in the region $x \ge 0$. At the seaward boundary $x = 0$ where $h_p = 0$ is assumed, the normalized incident wave train, $\eta_i = \eta'_i/H'$, is prescribed as a function of t and the normalized reflected wave train, $\eta_r = \eta'_r/H'$, is computed as a function of t from the characteristics advancing seaward.

The numerical model is compared with the three test runs denoted by runs P1, P2 and P3 conducted by Cox (1989). The upper boundary of the permeable gravel underlayer was located at $z'_t = (-d'_t + x'\tan\theta')$ with $d'_t = 0.40$ m and $\cot\theta' = 3$. Its lower boundary was situated at $z'_p = -d'_t$ for $0 \le x' \le 0.566$ m and $z'_p = -d'_t + (x' - 0.566)\tan\theta'$ for 0.566 m $\le x'$ where its thickness perpendicular to the impermeable base was $0.566\sin\theta' = 0.179$ m. The single layer of the gravel whose thickness was the median gravel diameter $d'_p = 2.1$ cm is regarded as the primary cover layer. The other input parameters associated with (4) are taken as $n_p = 0.48$, $\nu = 0.01$ cm^2/s at 20°C, $\alpha_0 = 1140$ and $\beta_0 = 2.7$.

The significant wave height H'_s and the mean period T'_m of the zero upcrossings of the measured incident wave train are taken as the height H' and the period T' used for the normalization of the governing equations. The values of $H' = H'_s$ and $T' = T'_m$ for the three runs are listed in Table 1. The other values listed in Table 1 are as follows: $\xi =$ surf similarity parameter based on H', T' and $\cot\theta' = 3$; $t_{max} =$ normalized duration of the measurement and computation; $H_{mo} =$ spectral estimate of the normalized significant wave height; $T_p =$ normalized spectral peak period; $\xi_p =$ surf similarity parameter based on the spectral parameters $H'_{mo} = H_{mo}H'$ and $T'_p = T_p T'$; and $f' =$ bottom friction factor estimated from the rough impermeable slope tests. The values of H_{mo} and T_p are obtained from the normalized incident wave spectrum $S_i(f_*)$ with $f_* =$ normalized frequency defined as $f_* = f'_i T'$ computed from $\eta_i(t)$ for $0 \le t \le t_{max}$ for each run. The frequency range of resolution of the measured incident and reflected waves based on three wave gages was $0.12 < f_* < 1.6$ for run P1, $0.15 < f_* < 2.0$ for run P2, and $0.19 < f_* < 2.6$ for run P3 (Kobayashi et al. 1990). Table 1 also lists the values of p_q and μ defined in (3) and (4). For these runs, the discharge velocity inside the permeable underlayer is generally small relative to the fluid velocity over the permeable slope, while the laminar flow resistance in the permeable underlayer is small as compared to the turbulent flow resistance.

Wurjanto and Kobayashi (1992) has shown that the numerical model can predict the time series and spectral characteristics of the measured reflected waves and waterline oscillations on the 1:3 permeable slope where the waterline meter measured the temporal variation of the elevation Z'_r above SWL of the intersection between the instantaneous free surface $z' = \eta'$ and the straight line $z' = (z'_b + \delta'_r)$ with $\delta'_r \simeq 2.75$ cm in the experiment. As a result, additional

Table 1: Three Test Runs Compared with Numerical Model

Run No.	H' (cm)	T' (sec)	ξ	t_{max}	H_{mo}	T_p	ξ_p	f'	p_q	μ
P1	6.85	1.08	1.72	170.98	1.01	1.09	1.88	0.05	0.043	0.074
P2	5.35	1.36	2.44	268.98	1.03	1.56	3.75	0.05	0.041	0.088
P3	4.57	1.74	3.39	210.01	1.06	1.58	5.22	0.10	0.038	0.104

computed results are presented hereafter to elucidate the interaction processes of irregular waves with the rough permeable slope with the thick permeable underlayer. In the following, the computed results for run P2 are shown as typical results but the computed results for runs P1 and P3 are similar unless stated otherwise.

Fig. 2 shows the computed spatial variations of η, u, $p_q q_b$ and $m_p = p_u h_p u_p$ at $t = 125.0$, 125.5 and 126.0 where the shaded area shown with the variation of η corresponds to the permeable underlayer. Comparison of the variations of η and u reveals the sequence of water uprushing and downrushing on the permeable slope from $t = 125.0$ to $t = 126.0$. The variations of $p_q q_b$ indicate water flowing into the permeable underlayer during wave uprush and water outflow in the region below the trough of the free surface. The variations of m_b show the flux inside the permeable underlayer which appears to be driven mainly by the hydrostatic pressure gradient related to $-\partial\eta/\partial x$ as is the case with the thin permeable underlayer (Kobayashi and Wurjanto 1990).

Fig. 3 shows the computed normalized spectra S_z^U and S_z^L of the upper and lower waterline oscillations, respectively. The upper waterline is taken as the normalized waterline elevation $Z_r = Z_r'/H'$ on the permeable slope, whereas the lower waterline corresponds to the normalized elevation above SWL of the intersection between the instantaneous water table $z = \eta$ and the straight line $z = (z_p + \delta_r'/H')$ with $\delta_r' = 2.75$ cm parallel to the impermeable slope $z = z_p$. Fig. 3 reveals that the permeable underlayer attenuates the high-frequency wave components significantly but damps the low-frequency wave components little as expected.

Fig. 4 shows the spatial variations of $\bar{m} = \overline{uh}$, $p_q \overline{q_b}$ and $n_p \overline{m_p} = p_q \overline{u_p h_p}$ where the overbar indicates the time averaging over $0 \leq t \leq t_{max}$. The time-averaged volume flux per unit horizontal area, $\overline{q_b}$, is into or out of the permeable underlayer above or below the still waterline located at $z_b = 0$, respectively, where $z_b = 0$ at $x = 1.22$ for run P2. Correspondingly, the time-averaged volume flux $\bar{m}$ and $\overline{m_p}$ above and inside the permeable underlayer are landward and seaward, respectively, in the vicinity of the still waterline. The overall mass balance requires that $\overline{q_b}$, $\bar{m}$ and $\overline{m_p}$ must approach zero at $x = 0$. In Fig. 4, $\bar{m}$ approaches a very small negative value at $x = 0$. This implies that the numerical model may not predict the small time-averaged quantities very accurately partly because they are small relative to the corresponding time-varying quantities.

COMPARISON BETWEEN PERMEABLE AND IMPERMEABLE SLOPES

The additional computed results for the 1:3 rough permeable slope are presented hereafter in comparison with the computed results for the corresponding impermeable slope without the permeable underlayer. These runs corresponding to runs P1, P2 and P3 are denoted by runs I1, I2 and I3. The numerical model for impermeable slopes was shown to be capable of predicting the time series and spectral characteristics of the reflected waves and waterline oscillations on the 1:3 rough impermeable slope (Kobayashi et al. 1990). The measured reflected waves and waterline oscillations on the permeable and impermeable slopes were compared by Kobayashi et al. (1991) who found it very difficult to generate identical incident wave trains for the permeable
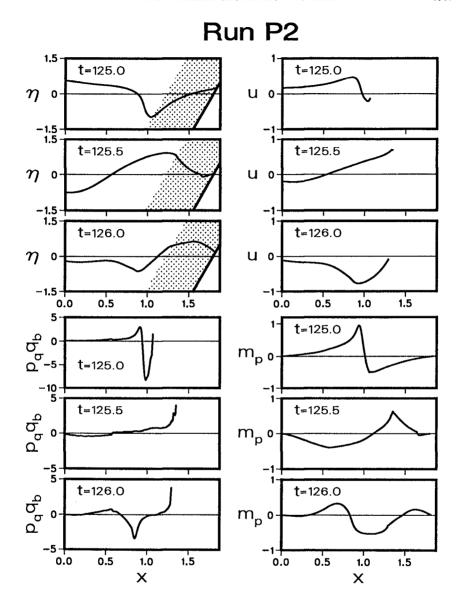
Run P2

Figure 2: Computed Spatial Variations of η, u, $p_q q_b$ and $m_p = p_u\, h_p\, u_p$ at $t = 125.0$, 125.5 and 126.0.
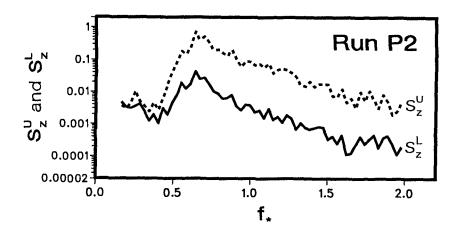
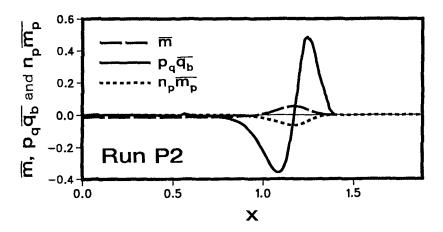Figure 3: Computed Spectra of Upper and Lower Waterline Oscillations Denoted by S_z^U and S_z^L, Respectively.

Figure 4: Time-Averaged Volume Fluxes $\bar{m}$, $p_q \overline{q_b}$ and $n_p \overline{m_p}$

Table 2: Computed Values of $\bar{r}$, $\overline{Z_r}$, R_s, R_{max} and N_{sc} for Permeable (P) and Impermeable (I) Slopes.

Run	$\bar{r}$		$\overline{Z_r}$		R_s		R_{max}		N_{sc}		N_s
No.	P	I	P	I	P	I	P	I	P	I	
1	0.09	0.20	0.06	0.12	0.57	0.91	1.01	1.48	1.16	0.49	2.29
2	0.15	0.55	0.05	0.14	0.78	1.52	1.11	2.20	1.49	0.38	1.78
3	0.26	0.66	0.05	0.11	0.94	1.72	1.85	3.24	1.43	0.45	1.52

and impermeable slope tests in a wave tank. In the present comparisons, the measured incident wave train for run PJ with J $=$ 1, 2 and 3 is specified as input to the computation for run IJ so that the incident wave trains for runs PJ and IJ become identical. Moreover, the numerical models allow us to examine the permeability effects on the quantities which are very difficult to measure.

Fig. 5 compares the computed spatial variations of η_{max}, $\bar{\eta}$ and η_{min} as well as u_{max}, $\bar{u}$ and u_{min} for runs P2 and I2 where the subscripts max and min indicate the maximum and minimum values with respect to t over $0 \le t \le t_{max}$. The presence of the thick permeable underlayer reduces the vertical range of the free surface elevation η and the magnitude of the depth-averaged horizontal velocity u on the slope. The wave setup $\bar{\eta}$ on the impermeable slope approaches η_{max} asymptotically since $\bar{h} = (\bar{\eta} - z_b) > 0$ in the region reached by uprushing water during $0 \le t \le t_{max}$, whereas the wave setup $\bar{\eta}$ on the permeable slope is connected to the wave setup inside the permeable underlayer. The negative value of $\bar{u}$ on the impermeable slope is related to undertow on a beach (Kobayashi et al. 1989), whereas the time-averaged fluxes for the permeable slope shown in Fig. 4 result in the positive value of $\bar{u}$ above the still waterline located at $x = 1.22$ for runs P2 and I2. This suggests that the permeability may affect the net cross-shore transport of gravel and sand.

Fig. 6 shows the computed reflection coefficient r as a function of the normalized frequency f_* for runs P2 and I2 where r is defined as $r = [S_r(f_*)/S_i(f_*)]^{1/2}$ with $S_r =$ normalized reflected wave spectrum calculated from $\eta_r(t)$ for $0 \le t \le t_{max}$. The computed values of r exceeding unity for run I2 may not be correct since r should not exceed unity unless additional waves propagating seaward are generated in the region $x > 0$. Fig. 6 indicates that the permeable underlayer dissipates the incident high-frequency wave components but damps the incident low-frequency wave components little. This is consistent with the computed results shown in Fig. 3. The average reflection coefficient $\bar{r}$ may be defined as $\bar{r} = [(m_o)_r/m_o]^{1/2}$ where $m_o =$ zero moment of $S_i(f_*)$; and $(m_o)_r =$ zero moment of $S_r(f_*)$. The computed values of $\bar{r}$ for the six runs listed in Table 2 increase with the increase of the surf similarity parameter ξ and ξ_p given in Table 1. Comparison of the values of $\bar{r}$ for the permeable and impermeable slopes for given ξ and ξ_p indicates that the thick permeable underlayer reduced $\bar{r}$ by a factor of more than two.
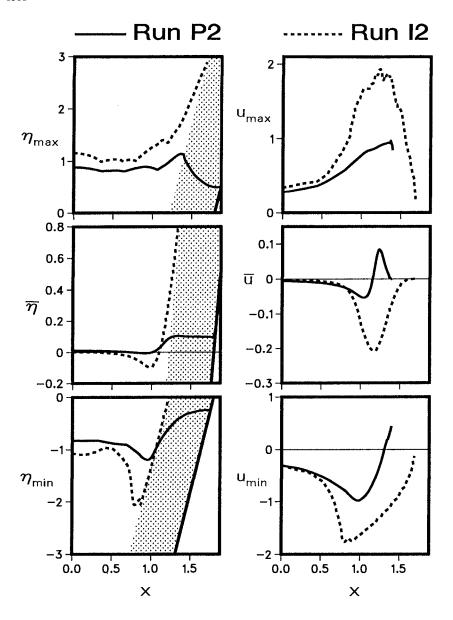
Figure 5: Computed Spatial Variations of η_{max}, $\bar{\eta}$ and η_{min} as well as u_{max}, $\bar{u}$ and u_{min}.
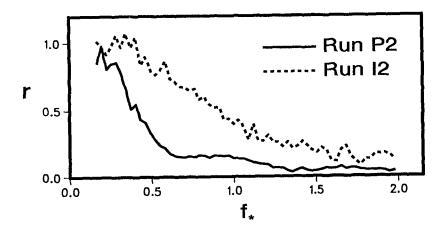
Figure 6: Reflection Coefficient r as a Function of Normalized Frequency f_*.

Fig. 7 shows the computed spectrum S_z^U of the normalized upper waterline elevation above SWL, $Z_r(t)$, for $0 \leq t \leq t_{max}$. The permeable underlayer reduces both high-frequency and low-frequency wave components unlike the computed results shown in Figs. 3 and 6. The interaction of uprushing and downrushing water on the impermeable slope seems to generate additional low-frequency wave components, whereas the permeable slope appears to absorb the incident waves with little water uprushing as shown in Fig. 2. The computed time series $Z_r(t)$ for $0 \leq t \leq t_{max}$ are also analyzed using the zero upcrossing method described by Kobayashi et al. (1990). Table 2 lists the computed values of $\overline{Z_r}$, R_s and R_{max} for the six runs where $\overline{Z_r}$ = time-averaged upper waterline elevation above SWL; R_s = normalized significant run-up defined as the average of the highest one- third run-up elevations above SWL; and R_{max} = maximum run-up elevation above SWL during $0 \leq t \leq t_{max}$. R_s and R_{max} increase with the increase of ξ and ξ_p given in Table 1. Moreover, the thick permeable underlayer reduces $\overline{Z_r}$, R_s and R_{max} by a factor of slightly less than two. Fig. 7 also shows the exceedance probability P as a function of R_p/R_s with R_p = normalized run-up corresponding to the specific value of P together with the Rayleigh distribution. The probability distribution of the normalized run-up, R_p/R_s is affected little by the permeable underlayer whose effect on run-up may be accounted for by R_s only.

Fig. 8 shows the computed spatial variations of $\bar{E}$, $\bar{F}$, $\overline{D_p}$ and $\bar{D} = (\overline{D_f} + \overline{D_B})$ for the flow over the permeable and impermeable slopes where $\bar{E}$ = normalized specific energy; $\bar{F}$ = normalized energy flux per unit width; $\overline{D_p}$ = normalized energy flux per unit horizontal area into the permeable underlayer which is zero for the impermeable slope; $\overline{D_f}$ and $\overline{D_B}$ = normalized rate of energy dissipation per unit horizontal area due to bottom friction and wave breaking, respectively. The one- dimensional energy equations and associated quantities have been explained by Kobayashi and Wurjanto (1990) and Wurjanto and Kobayashi (1992). For the permeable slope as compared to the impermeable slope, $\bar{E}$ does not increase much near the still waterline and the decrease of $\bar{F}$ starts from $x = 0$, while $\overline{D_p}$ is dominant as compared to $\bar{D}$ calculated from $\bar{D} = (-d\bar{F}/dx - \overline{D_p})$. For the impermeable slope with $\overline{D_p} = 0$, the comparison of $\overline{D_B}$ and $\overline{D_f}$ for runs I1, I2 and I3 indicates that $\overline{D_B}$ is dominant for run I1 and $\overline{D_f}$ is dominant for run I3, while $\overline{D_B}$ and $\overline{D_f}$ are equally important for run I2 as shown in Fig. 8.
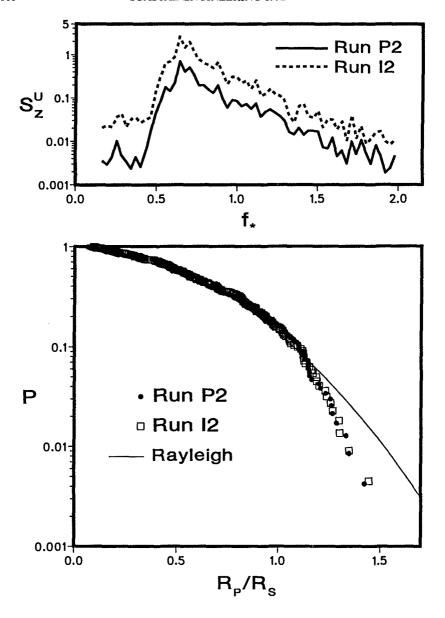
Figure 7: Computed Upper Waterline Spectrum S_z^U and Exceedance Probability P of Normalized Run-up R_p/R_s as Compared with Rayleigh Distribution.
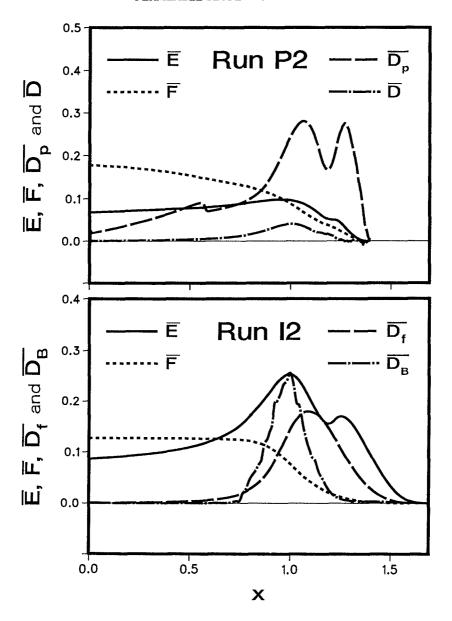
Figure 8: Time-Averaged Energy Fluxes and Dissipation Rates for Flow over Permeable and Impermeable Slopes.

Finally, the permeability effect on armor stability is examined. Kobayashi and Wurjanto (1990) expressed the hydraulic stability condition against sliding or rolling of an armor unit on a rough permeable slope in the form

$$N_s = H'(s-1)^{-1} \, (\rho s/W')^{1/3} \leq N_R(t, z_b) \tag{5}$$

where N_s = stability number; H' = characteristic wave height taken as the significant wave height H'_s, s = specific density of the armor units; ρ = fluid density; W' = median mass of the armor units; and N_R = armor stability function varying with the normalized time t and the armor location on the slope represented by z_b. For the gravel used in the experiment, $s =$ 2.7, $W' = 14.8$ g and $(W'/\rho s)^{1/3} = 1.76$ cm. The values of N_R at given t are computed in the region $h' \geq d'_p$ since the armor units are assumed to be fully submerged. The local stability number $N_{sx}(z_b)$ is defined as the minimum value of $N_R(t, z_b)$ at given z_b during $0 \leq t \leq t_{max}$. The critical stability number N_{sc} is defined as the minimum value of $N_{sx}(z_b)$ for the region $z_b \geq -d_t$. Table 2 lists the computed values of N_{sc} for the six runs together with the measured value of N_s for each run. Fig. 9 shows the spatial variations of $N_{sc}(z_b)$ for runs P2 and I2 with $N_s = 1.78$.

The numerical model predicts that the gravel units in the region $N_{sx} < N_s$ should slide or roll. Cox (1989) observed that loose gravel units on the permeable slope remained at their initial locations, whereas those on the impermeable slope were dislodged during the tests. Fig. 9 indicates the intense movement of loose gravel units in the wide region of the impermeable slope but the limited movement of loose gravel units on the permeable slope. As a result, the computed results are qualitatively consistent with the observations and the empirical formula of van der Meer (1988), although the sliding or rolling of gravel units may not result in the dislodgement of the gravel units from their initial locations. Fig. 9 also shows the spatial variations of η, u, du/dt and N_R at the time $t = t_{sc}$ when the minimum value of N_R with respect to z_b equals the critical stability number N_{sc}. For run I2 with $t_{sc} = 91.83$, the critical armor stability occurs during wave uprush when the landward fluid velocity and acceleration are very large. For run P2 with $t_{sc} = 197.66$, the critical armor stability occurs during wave downrush when the seaward fluid velocity and acceleration are large. It is noted that the stability analysis of Kobayashi and Wurjanto (1990) neglects the direct effect of q_b on the armor stability and may not be very accurate.

CONCLUSIONS

The numerical model developed for predicting the flow over a rough permeable slope and the flow inside a permeable underlayer has been used to elucidate the interaction processes of irregular waves with a thick permeable underlayer. The computed results have also been compared with those for the corresponding rough impermeable slope to examine the differences caused solely by the permeable underlayer. The thick permeable underlayer has been shown to increase the armor stability considerably and reduce the wave reflection and run-up significantly. Most of the computed results presented herein have been observed visually or described qualitatively by previous researchers. The numerical models yield quantitative data with high spatial and temporal resolutions. The numerical models also allow one to perform sensitivity analyses easily by changing only one input parameter in each numerical simulation. For example, it may be important for the design of berm breakwaters to examine the sensitivity of the computed results to the thickness, porosity and stone diameter of the permeable underlayer.
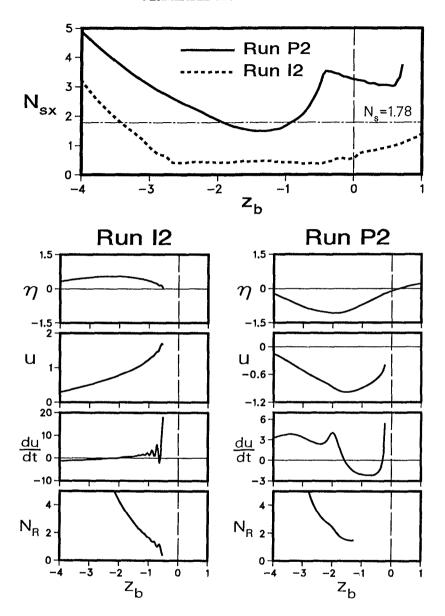
Figure 9: Spatial Variations of Local Stability Number N_{sx} and Flow Conditions at Time of Minimum Armor Stability.

REFERENCES

Cox, D.T. (1989). "Irregular wave reflection and runup on rough permeable slopes." Thesis for Master of Civil Engrg., Univ. of Delaware, Newark, DE.

Kobayashi, N., Cox, D.T. and Wurjanto, A. (1990). "Irregular wave reflection and run-up on rough impermeable slopes." *J. Wtrwy., Port, Coast. and Oc.Engrg.*, ASCE, 116(6), 708–726.

Kobayashi, N., Cox, D.T. and Wurjanto, A. (1991). "Permeability effects on irregular wave runup and reflection." *J. Coastal Res.*, 7(1), 127–136.

Kobayashi, N., DeSilva, G.S. and Watson, K.D. (1989). "Wave transformation and swash oscillation on gentle and steep slopes." *J. Geophys. Res.*, 94(C1), 951–966.

Kobayashi, N. and Wurjanto, A. (1990). "Numerical model for waves on rough permeable slopes." *J. Coastal Res.*, SI(7), 149–166.

Madsen, O.S. and White, S.M. (1975). "Reflection and transmission characteristics of porous rubble-mount breakwaters." *Tech. Rept. No. 207*, R. M. Parsons Lab., Mass. Inst. of Tech., Cambridge, Mass.

Van der Meer, J.W. (1988). "Rock slopes and gravel beaches under wave attack." Doctoral thesis, Delft Univ. of Tech., Delft, The Netherlands.

Wurjanto, A. and Kobayashi, N. (1992). "Irregular wave reflection and run-up on permeable slopes." *J. Wtrwy., Port, Coast. and Oc. Engrg.*, ASCE (submitted).